UC Davis
UC Davis Previously Published Works

Title

Fluonanobody-based nanosensor via fluorescence resonance energy transfer for ultrasensitive detection of ochratoxin A

Permalink

Authors

Su, Benchao
Zhang, Zhong
Sun, Zhichang
et al.

Publication Date

2022

DOI

Peer reviewed

Fluonanobody-Based Nanosensor *Via* Fluorescence Resonance Energy Transfer for Ultrasensitive Detection of Ochratoxin A

Benchao Su[a], Zhong Zhang[b], Zhichang Sun[a], Zongwen Tang[a], Xiaoxia Xie[a], Qi Chen[a], Hongmei Cao[a], Xi Yu[c], Yang Xu[d], Xing Liu[a,*], Bruce D. Hammock[e]

[a]School of Food Science and Engineering, Hainan University, Haikou 570228, China

[b]Engineering Research Center of High Value Utilization of Western Fruit Resources and College of Food Engineering and Nutritional Science, Shaanxi Normal University, Xi'an, Shanxi 710119, China

[c]Faculty of Medicine, Macau University of Science and Technology, Taipa, Macau 999078, China

[d]State Key Laboratory of Food Science and Technology, Nanchang University, Nanchang 330047, China

[e]Department of Entomology and Nematology and UCD Comprehensive Cancer Center, University of California, Davis, California 95616, USA

Abstract

Ochratoxin A (OTA) contamination in food is a serious threat to public health. There is an urgent need for development of rapid and sensitive methods for OTA detection, to minimize consumer exposure to OTA. In this study, we constructed two OTA-specific fluonanobodies (FluoNbs), with a nanobody fused at the carboxyl-terminal (SGFP-Nb) or the amino-terminal (Nb-SGFP) of superfolder green fluorescence protein. SGFP-Nb, which displayed better fluorescence performance, was selected as the tracer for OTA, to develop a FluoNb-based nanosensor (FN-Nanosens) *via* the fluorescence resonance energy transfer, where the SGFP-Nb served as the donor and the chemical conjugates of OTA-quantum dots served as the acceptor. After optimization, FN-Nanosens showed a limit of detection of 5 pg/mL, with a linear detection range of 5–5000 pg/mL. FN-Nanosens was found to be highly selective for OTA and showed good accuracy and repeatability in recovery experiments using cereals with various complex matrix environments. Moreover, the contents of OTA in real samples measured using FN-Nanosens correlated well with those from the liquid chromatography with tandem mass spectrometry. Therefore, this work

*To whom correspondence should be addressed: Prof. Dr. Xing Liu (X.L.), liu_xing307@163.com, xliu@hainanu.edu.cn.
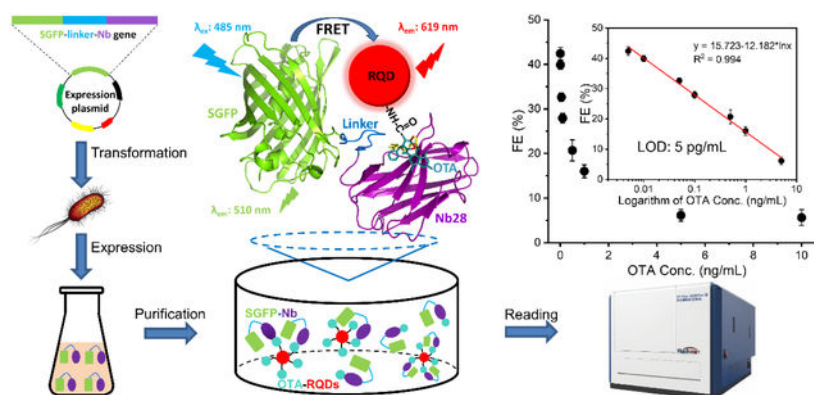
illustrated that the FluoNb is an ideal immunosensing tool and that FN-Nanosens is reliable for rapid detection of OTA in cereals with ultrahigh sensitivity.

Graphical abstract

Keywords

nanobody; superfolder green fluorescent protein; ochratoxin A; fluorescence resonance energy transfer; biosensor

1. Introduction

As a toxic secondary metabolite from several species of *Aspergillus* and *Penicillium*, ochratoxin A (OTA) contaminates various agro-products, such as beans, cereals, spices, coffee, milk, beer, wine, grape juice, and meat [1]. OTA can inhibit protein synthesis, disturb metabolic pathways, disrupt calcium homeostasis, and damage DNA in humans and animals. The potential human health risks of OTA exposure are related to nephrotoxicity, hepatotoxicity, immunotoxicity, teratogenicity, and carcinogenesis [2]. To reduce the exposure hazard of OTA, China [3] and the European Union [4] have set stringent regulatory levels of OTA in food, such as 2, 5, and 10 μg/kg for wine, cereal, and soluble coffee, respectively. Therefore, the development of rapid and sensitive detection technologies for OTA is very imperative to support the regulation of food safety.

Highly accurate and sensitive chromatography methods [5–7] are commonly used as confirmation methods for detection of OTA by the third testing organizations and government regulators of food safety. Nevertheless, the requirements for sophisticated instruments, laborious sample pretreatment, and specialized personnel limit their wide application by basic regulators or fields, for the rapid detection of hazardous materials in food. As alternatives to chromatography methods, immunoassays are very attractive options for high-throughput tests, because of their advantages of speediness, low cost, and high sensitivity. Immunoassays, including colorimetric immunoassays, chemiluminescent immunoassays, fluorescent immunoassays, bioluminescent immunoassays, and biosensors have been widely applied to detect various toxic low-molecular-weight compounds that are present in food and the environment [8–20]. A breakthrough was obtained upon application

of a combination of fluorescent immunoassays, biosensors, and fluorescence resonance energy transfer (FRET). The homogeneous reaction can eliminate the repetitive steps of incubation and washing, to expedite detection, thus improving the detection sensitivity [21].

FRET is triggered by narrowing the distance between two chromophores with overlapping spectra of emission and absorption spectra in the range of 1–10 nm; in this scenario, one chromophore is known as the donor while the other is known as the acceptor [22]. Chromophores with different characteristics mainly include organic dyes, quantum dots (QDs), and fluorescent proteins. The short fluorescence lifetime and photobleaching of the traditional organic dyes limit their application in reliable and long-term detection. Owing to their excellent properties, such as broad excitation spectra, narrow-band emission, and ease of surface modification, QDs are very attractive as a robust fluorescence nanomaterial [23, 24]. QDs have been used as both the donor and acceptor, where green QDs chemically labeled with the target analyte served as the donor and red QDs labeled with the target-specific antibody served as the acceptor [15]. However, the drawbacks of preparing antibody-QD conjugates using chemical coupling strategies, such as partial inactivation of the antibody and random coupling, are inevitable, which in turn influences the sensitivity, specificity, and repeatability of the method.

The discovery of green fluorescent protein (GFP) has piqued the wide interest of researchers in fluorescence proteins, because of their favorable fluorescence performance and stability [25]. Various GFP mutants with different optical properties have been generated, such as blue fluorescent protein, yellow fluorescent protein, and cyan fluorescent protein. Existing GFP variants are a group of ~26 kDa proteins that fluoresce green when exposed to light ranging from the blue to the ultraviolet spectra [26–28]. As reported, the better-folded variants of GFP are efficient fusion tags for proteins. Nevertheless, the folding yield and fluorescence intensity (FI) of GFP in fusion proteins cannot be guaranteed [29]. A recent novel mutant of GFP, namely superfolder GFP (SGFP), has attracted the wide attention of researchers owing to its excellent characteristics of high water solubility, hyperfluorescence, fast folding capacity, and good stability. Moreover, neither the misfolding of fusion partners nor the solubility of fusion can influence the fluorescence of SGFP fusion [30]. Thus, SGFP could be a very promising fluorescent tag for developing biosensors.

The nanobody (Nb) is the minimal functional antigen-binding fragment, which is mainly originates from the heavy-chain antibody of Camelidaes [31] and the new antigen receptor immunoglobulin of sharks [32]. Owing to the attractive characteristics of ease of prokaryotic expression with high yield, excellent water solubility, ease of genetic manipulation, and tolerance to harsh environments, various Nbs and Nb-derived fusion proteins have been generated to detect hazardous materials in food and the environment [9, 10, 33–37]. Nevertheless, there are very few reports on nanobody-fluorescence protein fusion (FluoNbs) for immune analysis, which is believed to be a very promising tool for immunoassays.

In this work, we constructed FluoNbs and investigated the feasibility of developing a FRET-mediated nanosensor designed using FluoNbs and QDs for the detection of OTA, as shown in Scheme 1. The influence of experimental parameters, such as reaction rate of donor and acceptor, reaction time, pH, methanol concentration, ion strength, and Tween-20

concentration on the proposed immunoassay was explored. The analytical performance of this method was assessed using OTA-spiked cereal samples and authentic samples and further confirmed using liquid chromatography with tandem mass spectrometry (LC-MS/MS). The proposed FRET immunoassay based on FluoNb exhibited high sensitivity and selectivity, with acceptable accuracy and precision, for detecting OTA in cereals. To our knowledge, there are very few reports on FRET-mediated nanosensors using FluoNb as the donor for detecting OTA and other low-molecular-weight compounds.

2. Materials and Methods

2.1 Materials and Instruments

Restriction enzymes and PrimeSTAR® HS DNA polymerase were supplied by Takara Biomedical Tech. Co. Ltd. (Beijing, China). The primers listed in Table S1 were synthesized by Sangon Biotech (Shanghai, China). Gluconic acid, *N, N*-dicyclohexyl carbodiimide (DCC), *N, N*-dimethyl formamide (DMF), and *N*-hydroxysuccinimide (NHS) were obtained from Aladdin (Shanghai, China). Standards of mycotoxins, including aflatoxin B_1 (AFB$_1$), deoxynivalenol (DON), fumonisin B_1 (FB$_1$), OTA, ochratoxin B (OTB), ochratoxin C (OTC), and zearalenone (ZEN) were purchased from Pribolab (Qingdao, China). The ZnCdSe/ZnS QDs modified with an amino group (RQD-NH$_2$, λ_{em}=614 nm) were supplied by Jiayuan Tech. (Wuhan, China). The recombinant vectors, pET25b-Nb28 encoding the Nb gene against OTA and pGEM-T-SGFP encoding the SGFP gene, were previously prepared in our laboratory. The remaining inorganic chemicals and organic solvents were of analytical grade or purity.

A spectral scanning multimode reader was used to scan the fluorescence spectra and UV–vis spectra (Infinite M200 Pro, Tecan, Switzerland). A PerkinElmer Frontier infrared spectrometer was used to analyze the Fourier transform infrared spectroscopy (FTIR) spectra (PerkinElmer, Waltham, MA, USA).

2.2 Construction of Recombinant Expression Vectors for FluoNbs

The vectors pET25b-Nb28 and pGEM-T-SGFP served as templates for the construction of the recombinant expression vectors of FluoNbs. Eight primers (SN-SF, SN-SR, SN-NF, SN-NR, NS-NF, NS-NR, NS-SF, and NS-SR), listed in Table S1, were designed to construct two FluoNbs fused with Nb28 at the carboxyl-terminal of SGFP (SGFP-Nb) or the amino-terminal of SGFP (Nb-SGFP). As shown in Scheme 1, the SGFP fragment was amplified using polymerase chain reaction (PCR) with pGEM-T-SGFP as the template; the primer pair of SN-SF and SN-SR containing the *Hind*III restriction enzyme site and linker sequence was used for SGFP-Nb, while the primer pair of NS-SF and NS-SR containing linker sequence and *Not*I restriction enzyme site was used for Nb-SGFP. The Nb fragment was obtained from pET25b-Nb28 as a template, using PCR with the primer pair of SN-NF and SN-NR containing linker sequence and *Not*I restriction enzyme site for SGFP-Nb, and the pair of NS-NF and NS-NR containing the *Hind*III restriction enzyme site and linker sequence for Nb-SGFP. The PCR conditions used have been shown in the Supplementary Material.

After identification using DNA agarose gel electrophoresis, the fragments SGFP and Nb were purified with a cycle-pure kit (Omega, Guangzhou, China) and subjected to splicing of both genes using sequence overlap extension PCR (SOE PCR). Briefly, the SGFP and Nb were spliced together using a two-step PCR, as shown in the Supplementary Material, where both fragments served as the primers for each other. Subsequently, the products were applied to amplify the SGFP-$(G_4S)_3$-Nb fragment with the primer pair of SN-SF and SN-NR, and the Nb-$(G_4S)_3$-SGFP fragment with the pair of NS-NF and NS-SR. The PCR conditions used have been listed in the Supplementary Material.

The obtained SGFP-$(G_4S)_3$-Nb and Nb-$(G_4S)_3$-SGFP fragments were purified and digested with the restriction enzymes *Hind*III and *Not*I. After digestion, the fragments were purified and inserted into a similarly digested pET25b vector, at a molar ratio of 3:1, using T4 DNA ligase (New England Biolabs, Beverly, MA, USA), followed by transformation of the ligated product into competent *E. coli* DH5α cells. The transformed bacteria were then cultivated on Luria-Bertani solid medium supplemented with ampicillin (50 μg/mL), following which individual bacterial colonies were randomly selected for nucleic acid sequencing.

2.3 Expression and Characterization of Recombinant FluoNbs

E. coli BL21(DE3) cells containing the verified recombinant vectors after transformation were used for auto-induction, as described previously [38]. After auto-induction, the bacterial cells were collected from the medium by centrifugation ($5000 \times g$, 15 min), followed by freezing at $-80°C$ and resuspension in lysis buffer (43.8 mM NaH_2PO_4, 300 mM NaCl, 20 mM imidazole, pH 8.0) supplemented with 1 mM phenylmethanesulfonyl fluoride and 1 mg/mL lysozyme. After ultrasonication and centrifugation, the supernatant containing soluble FluoNbs was separated from the lysed bacteria. Subsequently, the supernatant was passed through a 0.45 μm filter and transferred to an affinity column loaded with nickel-nitrilotriacetic acid agarose for histidine-tagged protein purification, as described previously [33]. The eluate from the affinity column was dialyzed at 4°C for 72 h in phosphate buffer (PB, 50 mM, pH 7.8) and frozen at $-20°C$ before use. The expression and purity of FluoNbs were analyzed using sodium dodecyl sulfate-polyacrylamide gel electrophoresis (SDS-PAGE), and the concentrations of FluoNbs were determined using a NanoDrop® 1000 spectrophotometer (Thermo Fisher Scientific, Wilmington, DE, USA). The activities of the Nb partner in SGFP-Nb and Nb-SGFP were determined using a direct competitive enzyme-linked immunosorbent assay (ELISA), as reported previously [8]. The fluorescence intensities at 510 nm of the SGFP partner in both the FluoNbs were recorded upon excitation at the wavelength of 485 nm.

2.4 Preparation and Characterization of the OTA-RQD Conjugates

OTA was immobilized on RQD-NH_2 using the DCC/NHS method, to prepare the OTA-RQD conjugates (OTA-RQDs), as described below. Briefly, a mixture of 1.32 μg DCC and 0.38 μg NHS in 100 μL of DMF was incubated with different amounts of OTA standards (0.8, 1.6, and 3.2 nmol) by shaking (30°C, 2 h) in the dark, to prepare the active esters of OTA. The resultant solution was added dropwise to 500 μL RQD-NH_2 solution (0.4 μM in 0.2 M borate buffer, pH 7.4) and incubated at room temperature for 90 min. The OTA-RQDs were blocked by incubation with 0.2 μmol gluconic acid for 60 min, followed by collection

through two rounds of centrifugation (27000 × *g*, 30 min). The OTA-RQDs were redissolved in borate buffer and stored at 4°C.

2.5   Measurements using FluoNb-Based Nanosensor

Measurements using FluoNb-based nanosensor (FN-Nanosens) *via* FRET were conducted as described below. First, a mixed solution of 10 μL SGFP-Nb (10 μg/mL), 10 μL OTA-RQDs, and 180 μL PB (50 mM, pH 7.8) was transferred to a black 96-well microtiter plate (Corning Incorporated, Corning, NY, USA). Subsequently, 20 μL of OTA standard solution ranging from 0 to 1000 pg/mL in 50% methanol-PB solution was added for competitive reaction (37°C, 10 min). Finally, the FI of the solution at 619 nm (λ_{em} of OTA-RQDs) was determined upon excitation at 485 nm (λ_{ex} of SGFP-Nb). The standard curve was plotted by fitting the fluorescence enhancement rate (FE) *versus* the logarithm of the OTA concentration for the quantitative analysis of OTA. The equation for the calculation of FE value is FE = ($FI_{D\&A}$-FI_D)/FI_D, in which $FI_{D\&A}$ and FI_D represent the fluorescence intensity at 619 nm in the presence and absence of OTA-RQDs, respectively.

2.6   Selectivity of the FluoNb-Based Nanosensor

The OTA standards were replaced with six substitutes, AFB_1, DON, FB_1, OTB, OTC, and ZEN, at two concentrations - 0.01 and 1 ng/mL, and subjected to measurement using FN-Nanosens. The calculated FEs were used to evaluate the selectivity of FN-Nanosens.

2.7   Method Validation in a Complex Environment

Cereal samples, including barley, oats, rice, and wheat, were pre-treated and tested to investigate the effectiveness of the proposed FN-Nanosens, as follows. First, 1 g of milled cereal sample was immersed in 5 mL of PB (50 mM, pH 7.8) with 50% methanol (v/v), followed by ultrasonic extraction for 15 min. After 15 min of centrifugation (8000 × *g*, 4°C), the supernatant was transferred and filtered through a syringe filter of 0.45 nm, and the prepared filtrate samples were tested using FN-Nanosens. To validate the effectiveness of FN-Nanosens, authentic cereal samples tested using FN-Nanosens were further analyzed using LC-MS/MS [33].

3.   Results and Discussion

3.1   Expression and Characterization of the Recombinant FluoNbs

Recombinant plasmids with the inserted fragments of SGFP-$(G_4S)_3$-Nb and Nb-$(G_4S)_3$-SGFP were confirmed using colony PCR (Figure S1–S3) and nucleic sequencing. Recombinant *E. coli* BL21(DE3) cells were constructed to express FluoNbs (Nb-SGFP and SGFP-Nb), and the expression of FluoNbs was evaluated using SDS-PAGE (Figure 1A). A predicted band of approximately 47.2 kDa for FluoNbs was present in the total bacterial protein after auto-induction, while it was absent before the induction (lanes 1 and 2 in both Figure 1A up and down). Moreover, a single clear band of approximately 47.2 kDa was observed in the eluate of the supernatant after purification (lane 3 in Figure 1A up and down), indicating that the FluoNbs were well prepared and of high purity. The yields of soluble Nb-SGFP and SGFP-Nb were calculated to be 10.5 mg/L and 46.5 mg/L, respectively, after quantification. The activity of Nb in both the FluoNbs was tested using

indirect competitive ELISA. As seen in Figure 1B, Nb-SGFP and SGFP-Nb showed similar antigen-binding activities. No significant variation was observed between the half maximal inhibitory concentration (IC_{50}) values (0.67 and 0.66 ng/mL) of both the FluoNbs, which were similar to the IC_{50} (0.64 ng/mL) of the original unfused Nb [8]. Therefore, the fusion format of SGFP at the N- or C-terminus of Nb seemed to have no significant influence on the antigen-recognition capacity of the antibody. The FI of 100 μL/well of each FluoNb (0.039, 0.078, 0.156, 0.312, 0.624, 1.248, 2.496, 4.992, 9.984, and 19.968 pmol/assay) was tested, and no significant difference was detected in the FI of either FluoNb (Figure 1C). These results could mainly be attributed to the excellent flexibility of the linker domains between Nb and SGFP, which is useful for facilitating the correct folding of Nb and SGFP in both the FluoNbs. The length of the linker peptide $(G4S)_3$ of FluoNbs was designed to contain 15 amino acids encoded by 45 bp. By comparison, the Nb-SGFP had a 1.5-fold longer linker sequence than the SGFP-Nb, since the hinge region containing eight amino acids (24 bp) at the C-terminus of Nb is a flexible sequence, which can function as an additional linker in the Nb-SGFP, in which the Nb is fused at the N-terminus of SGFP. Because of the relatively higher FI and soluble expression yield, SGFP-Nb was selected for further research. The thermal stability of SGFP-Nb was evaluated upon incubation at room temperature, 4°C, and −20°C for various time-periods, as described in the Supplementary Material. By comparison, preservation at −20°C was found to be the most effective means to ensure stable activity of SGFP-Nb, and no significant variations were observed even after incubation for 336 h (14 d) at −20°C, as shown in Figure S4.

3.2 Preparation and Characterization of the OTA-RQDs

To prepare the OTA-RQDs, four groups of OTA and $RQD-NH_2$ with input molar ratios of 5:1, 10:1, 15:1, and 20:1 were first tested. The excess OTA was quantified as previously described [8], and the coupling ratio for OTA was calculated according to the equation: coupling ratio (%) = $[(n_{input\ OTA} − n_{excess\ OTA})/n_{input\ OTA}] \times 100\%$. As shown in Table S2, the coupling ratios for OTA were determined as 74.51%, 76.83%, 74.76%, and 61.42%, which meant that one $RQD-NH_2$ particle was averagely immobilized with 3.73, 7.68, 11.21, and 12.28 OTA molecules, respectively. After labeling with OTA, the emission peak of the RQDs was characterized by a redshift from 615 nm to 619 nm, as shown in Figure 2A. The FI of OTA-RQDs at 619 nm upon excitation at 485 nm increased upon increasing the input molar ratio of $OTA/RQD-NH_2$ from 5:1 to 10:1, whereas it varied very slightly when the ratio was continuously increased. This result could mainly be ascribed to that the superfluous immobilization of OTA, which induces the surface effect of the RQDs [39]. Moreover, the FI at 430 ± 2 nm of the OTA-RQDs (λ_{ex}=365 nm) increased with increasing reactant mole ratio of $OTA/RQD-NH_2$, indicating that an increasing number of OTA molecules were immobilized on $RQD-NH_2$.

The FTIR spectra of free $RQD-NH_2$, OTA, and OTA-RQDs were further tested to confirm the coupling of OTA to $RQD-NH_2$ (Figure 2B and Table S3). The free $RQD-NH_2$ showed a characteristic N–H stretching peak at 3448.47 cm^{-1} in the FTIR spectrum. The free OTA exhibited a C=O stretching peak of carboxyl at 1605.90 cm^{-1}, which was mainly caused by the hydrogen bond formed between the oxhydryl and amino groups of OTA and the conjugative effect from the π bonds in benzene rings around the carboxyl of OTA. In

addition, a peak of O–H stretching for the carboxyl of free OTA was observed at 3436.34 cm^{-1}. After conjugation, the above peaks were absent from the OTA-RQDs. Moreover, a new N–H stretching peak at 3516.57 cm^{-1} and a new C=O peak at 1650.78 cm^{-1} that was partially covered by the strong C=O stretching peak at 1720.33 cm^{-1} appeared in the OTA-RQDs, indicating that a new amide I group was generated by dehydration condensation between the carboxyl of OTA and the amino group of RQD-NH$_2$. Thus, the results demonstrated that OTA was successfully coupled with RQD-NH$_2$.

3.3 Construction of the FluoNb-Based Nanosensor

To verify the feasibility of developing an FRET-mediated nanosensor using FluoNb (SGFP-Nb) and OTA-RQDs, the fluorescence spectra of SGFP-Nb and OTA-RQDs-10, and the absorption spectrum of OTA-RQDs-10 were first determined, where the OTA-RQDs-10 denotes the OTA-RQD conjugate prepared with a 10:1 input molar ratio of OTA and RQD-NH$_2$. As seen in Figure 3A, the UV–vis absorption spectrum of OTA-RQDs-10 exhibited a highly overlapped area with the fluorescence emission spectrum of SGFP-Nb in the range of 470–628 nm. Moreover, the emission spectra of SGFP-Nb and OTA-RQDs-10 were apart from each other, with no significant effective overlap. These results confirmed the prerequisite for the occurrence of FRET between SGFP-Nb (donor) and OTA-RQDs (acceptor). The fluorescence lifetimes of SGFP-Nb in the presence and absence of OTA-RQDs were determined to confirm the fluorescence quenching mechanism of SGFP-Nb by OTA-RQDs (Figure 3B). After incubation with the OTA-RQDs, the fluorescence lifetime of SGFP-Nb declined significantly with the τ_1 decreasing from 2.57 ns to 0.92 ns and the τ_2 from 5.13 ns to 2.58 ns. Moreover, the estimated maximum FRET distance between SGFP-Nb and OTA-RQDs (9.31 nm) was smaller than the calculated Forster distance (R_0 = 12.84 nm), as described in the Supplementary Material. Thus, FRET was proved to mainly contribute to the fluorescence quenching of SGFP-Nb by OTA-RQDs. Furthermore, the negative staining transmission electron microscopy (TEM) was also conducted to analyze the morphology of both SGFP-Nb and OTA-RQDs [40]. As shown in Figure 3C, we observed not only the free OTA-RQDs and SGFP-Nb with regular morphology, but also the OTA-RQDs/SGFP-Nb immunocomplex with irregular morphology in the mixture of OTA-RQDs and SGFP-Nb. This phenomenon demonstrated that the FRET in this case was triggered by a specific antigen-antibody interaction between SGFP-Nb and OTA-RQDs.

Because the bioconjugation mole ratio of SGFP to Nb in the donor was fixed at 1:1, it was necessary to optimize the coupling molar ratio between OTA and RQD-NH$_2$ for optimal energy transfer efficiency. Figure 3D shows that the FE increased with increasing molar ratio from 5:1 to 10:1. However, it gradually decreased as the molar ratio increased from 10:1 to 20:1. This phenomenon could be ascribed to the enhanced hydrophobicity of RQD-NH$_2$ induced by the excessively immobilized OTA, which can affect the interaction between SGFP-Nb and OTA-RQDs. Because of the highest FE, the SGFP-Nb/OTA-RQDs-10 group was selected as the optimal donor-acceptor pair for further research.

3.4 Optimization of the FluoNb-Based Nanosensor

To determine the optimum detection performance of FN-Nanosens, various experimental conditions were optimized in sequence. First, the quenching efficiencies at different input

molar ratios of donor SGFP-Nb and acceptor OTA-RQDs-10 were tested. As seen in Table S4, the quenching efficiency dramatically increased with an increase in the reactant mole ratio from 1:1 to 3:1, and slightly declined when the ratio was continuously increased to 5:1. Therefore, the optimum input molar ratio of SGFP-Nb/OTA-RQDs-10 was determined to be 3:1 for the highest quenching efficiency of $(38.09 \pm 1.42)\%$. Second, the influence of different competitive reaction times on method performance was evaluated. As shown in Figure 4A, the FE increased sharply from 10.04% to 39.25%, with a competitive reaction time in the range of 0–5 min. However, it remained stable when the time was extended from 5 to 30 min. Hence, the optimal competitive reaction time was determined to be 5 min. Four key factors of the reaction solution that could influence the antibody-antigen interaction were further assessed. As seen in Figure 4B, a rapid increase from 25.6% to 41.4% in the FE was observed in the pH values ranging from 6.2 to 7.0, while there was a marginal increase in the FE, from 41.4% to 42.78%, when the pH was in the range of 7.0–7.8. However, it dropped rapidly to 37.82% as the pH increased to 8.6. These results indicated that the antibody-antigen interaction of the proposed FN-Nanosens was highly sensitive to the solution pH; the optimum pH was confirmed to be 7.8, because of the observation of the highest FE at this pH. Methanol is a commonly used organic solvent for the analysis of OTA and other lipophilic analytes. As shown in Figure 4C, the FE varied when the methanol concentration of the reaction system ranged from 0% to 30%, and the highest FE of 42.9% was obtained with 2.5% methanol. To assess the influence of ion strength on assay performance, PB solutions supplemented with various concentrations of sodium chloride (NaCl) (0–200 mM) were applied to FN-Nanosens. As seen in Figure 4D, the FE increased to a maximum of 48.53% when the concentration of NaCl was increased to 20 mM. Nevertheless, a remarkable reduction in the rate was observed upon further supplementation with NaCl. Hence, a PB solution with an ion strength of 20 mM of NaCl was selected. The concentration of the non-ionic surfactant Tween-20 of the assay system was optimized, and the optimum performance of the proposed method was determined using 0.05% Tween-20 (Figure 4E). Thus, the optimal experimental conditions after optimization were as follows: input molar ratio of SGFP-Nb/OTA-RQDs-10, 3:1; competitive reaction time, 5 min; pH, 7.8; methanol concentration, 2.5%; ion strength, 20 mM NaCl; Tween-20 concentration, 0.05%.

3.5 Detection Performance of the FluoNb-Based Nanosensor

Based on the optimum experimental parameters, the detection performance of the developed FN-Nanosens was investigated. Fluorescence spectra were first scanned for the mixed SGFP-Nb, OTA-RQDs-10, and a series of standard solutions of OTA (0–10000 pg/mL). As seen in Figure 5A, the FI of the mixture with a fixed excitation wavelength of 485 nm declined at 619 nm (λ_{em} of OTA-RQDs-10) and increased at 510 nm (λ_{em} of SGFP-Nb) with increasing OTA concentration. When the concentration of OTA in the mixture reached 10000 pg/mL, no significant variation was observed in the FI at 510 nm of the mixture and the control group of 0.5 μg/mL SGFP-Nb. In addition, both control groups of OTA-RQDs-10 and 10000 pg/mL OTA showed no emission at 510 nm upon excitation at 485 nm. Therefore, these results indicated the competitive reaction of OTA and OTA-RQDs-10 for specific binding to SGFP-Nb, which could cause a decrease in FE, as shown in Figure 5B. A remarkable linear relationship (R^2=0.994) was obtained between the FE and logarithmic

concentration of OTA (5–5000 pg/mL). Moreover, FN-Nanosens had a limit of detection (LOD) of 5 pg/mL, which was defined as the mean value of 20 blanks plus three standard deviations (SDs) of the blanks. As observed in Figure 5A, after deducting the FI of OTA-RQDs-10, which acted as the blank control, the valid change in FI for quantitative analysis ranged from approximately 2 K to 0.5 K, which is equal to 3/4th of the total intensity, indicating efficient application of FN-Nanosens.

For comparison, we also developed an enhanced green fluorescence protein-nanobody fusion protein (EGFP-Nb) to replace SGFP-Nb for the FRET-mediated nanosensor (EN-Nanosens). The construction (primers listed in Table S5) and characterization of EGFP-Nb are detailed in the Supplementary Material. Based on the optimum experimental parameters, the EN-Nanosens showed a 4-fold higher LOD of 20 pg/mL, as compared to that of FN-Nanosens (Figure 5C). This could mainly be attributed to the higher FI of SGFP compared with that of EGFP, which can generate higher quantum yield and energy transfer efficiency, although the EGFP-Nb showed a higher sensitivity in the colorimetric immunoassay than the SGFP-Nb (Figure S5). Compared to other reported highly sophisticated equipment- and nanotechnology-based detection methods for OTA, the proposed FN-Nanosens exhibited significant superiority in sensitivity, speed, and linear detection range, as shown in Table S6. Compared with the FRET-mediated immunosensor based on the Nb-RQDs/OTA-GQDs pair [15], the currently proposed method is more cost-efficient and eco-friendly for the use of cloneable SGFP-Nb by biosynthesis instead of the Nb-RQD conjugate by chemical labeling (Table S7). Figure 5D indicates that negligible decreases in the FE were measured when the substitutes of OTA listed in Figure 5E were added, as compared to when OTA was added. Thus, FN-Nanosens was highly selective for OTA, as demonstrated here.

To analyze the interactions between SGFP-Nb and three ochratoxins (OTA, OTB, and OTC) for explaining the good selectivity of SGFP-Nb for OTA, molecular docking was conducted using the CDOCKER protocol of Discovery Studio software, as described in the Supplementary Material. Figure 6 displays the molecular docking results of SGFP-Nb and the three ochratoxins. There are several forces involved in the binding sites between the Nb subunit and three ochratoxins, including hydrogen bonds (conventional hydrogen bonds and carbon hydrogen bonds), hydrophobic interactions (alkyl and pi-alkyl interaction), van der Waals, and pi-lone pairs. As seen in Figure 6A–B, Val97 and Tyr99 in the CDR3 region of the Nb subunit formed alkyl and pi-alkyl interactions with OTA, respectively. Gly10 and Gly11, near the CDR3 region of the Nb subunit, served as H bond acceptors and formed conventional hydrogen bonds with OTA. This finding was consistent with a previous study, which demonstrated that CDR3 is vital for the interaction between the antigen and Nb [41]. In addition, the Gln113 in FR4 region formed a carbon hydrogen bond with OTA. In addition to these interactions, the relatively large van der Waals areas might contribute to the docking of the Nb subunit and OTA as well. Figure 6C–D indicates that the Gly12 and Leu13 in the CDR1 region of the Nb subunit formed a conventional hydrogen bond and alkyl interaction, respectively, with OTB. As observed in Figure 6E–F, the interaction of Nb28 and OTC was only in terms of van der Waals interactions. These differences in interactions could contribute to the sensitivity variations of SGFP-Nb against OTA, OTB, and OTC. The energy of the molecular docking is summarized in Table 1. In the CDOCKER module of DS, the –CDOCKER interaction energy was used to evaluate the docking results.

A higher score indicates better binding between the two molecules [42]. The –CDOCKER interaction energies of the three ochratoxins decreased in the following order: OTA, OTC, and OTB. More interactions and higher –CDOCKER interaction energy between the binding sites of the Nb subunit with OTA than with OTB or OTC could be interpreted as higher binding specificity of SGFP-Nb against OTA.

3.6 Method Validation in the Complex Environment of the Food Matrix

Based on its favorable analytical performance, the effectiveness of FN-Nanosens was further evaluated in a complex environment using practical cereal samples. The accuracy and repeatability of FN-Nanosens were tested through spiking and recovery experiments. Cereal samples previously confirmed as negative using LC-MS/MS were used to generate various increasing levels of the OTA standard (0.02, 0.2, and 2 μg/kg). The separated supernatants containing OTA after extraction were directly diluted to eliminate matrix effects (10-, 25-, 40- and 100-fold dilutions for rice, barley, wheat, and oats, respectively, as shown in Figure S6), as described in the Supplementary Material, and then detected using FN-Nanosens. Table 2 shows that the developed method has a mean recovery rate of 70%–109% for intra-assay and 73%–106% for inter-assay, and corresponding relative standard deviation (RSD) of 4%–16% and 3%–16%, respectively, confirming the high accuracy and repeatability of FN-Nanosens. Furthermore, the OTA contents of the 13 positive cereal samples tested, as measured using FN-Nanosens, were linear with those determined using LC-MS/MS (Table 3 and Figure S7). Therefore, the above results demonstrated the applicability and reliability of FN-Nanosens for rapid detection of OTA in cereals, with ultrahigh sensitivity and good selectivity.

4. Conclusions

In the present study, we report a novel immunosensing probe, the FluoNb (SGFP-Nb), and a rapid, ultrasensitive, and selective FN-Nanosens *via* FRET from SGFP to QDs for detecting OTA in cereals. Owing to the unique features of Nb and SGFP, FN-Nanosens can be more widely applied than the other immunoassay formats. As demonstrated here, Nb allows for ease of genetic manipulation and expression in the prokaryotic system, and the high quantum yield of SGFP is beneficial for improving the FRET efficiency and obtaining higher detection sensitivity. We also demonstrated that SGFP fusions could be very promising immune tracers for low-molecular-weight analytes. The SGFP fusion technology could produce a cloneable SGFP-Nb probe with a fixed reporter/probe molar ratio of 1:1. It can also replace the QDs chemically labeled with Nbs, thus making FN-Nanosens economical and eco-friendly. Moreover, FN-Nanosens integrates the advantages of no-wash, one-step detection, and high detection sensitivity, which are attributed to their homogeneous detection mode. Hence, this work provides a new detection mode for the analysis of ultralow levels of small-molecule contaminants.

Supplementary Material

Refer to Web version on PubMed Central for supplementary material.

Acknowledgments

References

[1]. Patriarca A, Fernández Pinto V, Prevalence of mycotoxins in foods and decontamination, Current Opinion in Food Science, 14 (2017) 50–60.

[2]. Tao Y, Xie S, Xu F, Liu A, Wang Y, Chen D, Pan Y, Huang L, Peng D, Wang X, Yuan Z, Ochratoxin A: Toxicity, oxidative stress and metabolism, Food and Chemical Toxicology, 112 (2018) 320–331. [PubMed: 29309824]

[3]. NHC PRC, The maximum limits of mycotoxins in food, in: National Health Commission of the People's Republic of China (Ed.), 2017, pp. 1–10.

[4]. E.C. Regulation, Commission regulation (EC) no. 1881/2006 of 19 December 2006 setting maximum levels for certain contaminants in foodstuffs, Official Journal of the European Union, L364 (2006) 5–18.

[5]. Moez E, Noel D, Brice S, Benjamin G, Pascaline A, Didier M, Aptamer assisted ultrafiltration cleanup with high performance liquid chromatography-fluorescence detector for the determination of OTA in green coffee, Food Chemistry, 310 (2020) 125851. [PubMed: 31767477]

[6]. Zhang X, Li M, Cheng Z, Ma L, Zhao L, Li J, A comparison of electronic nose and gas chromatography–mass spectrometry on discrimination and prediction of ochratoxin A content in Aspergillus carbonarius cultured grape-based medium, Food Chemistry, 297 (2019) 124850. [PubMed: 31253256]

[7]. Campone L, Rizzo S, Piccinelli AL, Celano R, Pagano I, Russo M, Labra M, Rastrelli L, Determination of mycotoxins in beer by multi heart-cutting two-dimensional liquid chromatography tandem mass spectrometry method, Food Chemistry, 318 (2020) 126496. [PubMed: 32146309]

[8]. Liu X, Tang Z, Duan Z, He Z, Shu M, Wang X, Gee SJ, Hammock BD, Xu Y, Nanobody-based enzyme immunoassay for ochratoxin A in cereal with high resistance to matrix interference, Talanta, 164 (2017) 154–158. [PubMed: 28107910]

[9]. Sun Z, Lv J, Liu X, Tang Z, Wang X, Xu Y, Hammock BD, Development of a Nanobody-AviTag Fusion Protein and Its Application in a Streptavidin–Biotin-Amplified Enzyme-Linked Immunosorbent Assay for Ochratoxin A in Cereal, Analytical Chemistry, 90 (2018) 10628–10634. [PubMed: 30092629]

[10]. Wang F, Li Z, Yang Y, Wan D, Vasylieva N, Zhang Y, Cai J, Wang H, Shen Y, Xu Z, Hammock BD, Chemiluminescent enzyme immunoassay and bioluminescent enzyme immunoassay for tenuazonic acid mycotoxin by exploitation of nanobody and nanobody–nanoluciferase fusion, Analytical Chemistry, 92 (2020) 11935–11942. [PubMed: 32702970]

[11]. Dong J, Li Z, Wang Y, Jin M, Shen Y, Xu Z, Abd El-Aty AM, Gee SJ, Hammock BD, Sun Y, Wang H, Generation of functional single-chain fragment variable from hybridoma and development of chemiluminescence enzyme immunoassay for determination of total malachite green in tilapia fish, Food Chemistry, 337 (2021) 127780. [PubMed: 32799164]

[12]. Wang X, Wang Y, Wang Y, Chen Q, Liu X, Nanobody-alkaline phosphatase fusion-mediated phosphate-triggered fluorescence immunoassay for ochratoxin a detection, Spectrochimica Acta Part A: Molecular and Biomolecular Spectroscopy, 226 (2020) 117617.

[13]. Zhou K, Wang Z, Luo L, Dong Y, Yang J, Lei H, Wang H, Shen Y, Xu Z, Development of Cu(II)/Cu(I)-induced quantum dot-mediated fluorescence immunoassay for the sensitive determination of ethyl carbamate, Microchimica Acta, 187 (2020) 533. [PubMed: 32870401]

[14]. Li Z, Wang Y, Vasylieva N, Wan D, Yin Z, Dong J, Hammock BD, An ultrasensitive bioluminescent enzyme immunoassay based on nanobody/nanoluciferase heptamer fusion for the

detection of tetrabromobisphenol A in sediment, Analytical Chemistry, 92 (2020) 10083–10090. [PubMed: 32559059]

[15]. Tang Z, Liu X, Su B, Chen Q, Cao H, Yun Y, Xu Y, Hammock BD, Ultrasensitive and rapid detection of ochratoxin A in agro-products by a nanobody-mediated FRET-based immunosensor, Journal of Hazardous Materials, 387 (2020) 121678. [PubMed: 31753666]

[16]. He Y, Tian F, Zhou J, Zhao Q, Fu R, Jiao B, Colorimetric aptasensor for ochratoxin A detection based on enzyme-induced gold nanoparticle aggregation, Journal of Hazardous Materials, 388 (2020) 121758. [PubMed: 31796354]

[17]. Altunbas O, Ozdas A, Yilmaz MD, Luminescent detection of Ochratoxin A using terbium chelated mesoporous silica nanoparticles, Journal of Hazardous Materials, 382 (2020) 121049. [PubMed: 31470297]

[18]. Pagkali V, Petrou PS, Makarona E, Peters J, Haasnoot W, Jobst G, Moser I, Gajos K, Budkowski A, Economou A, Misiakos K, Raptis I, Kakabakos SE, Simultaneous determination of aflatoxin B1, fumonisin B1 and deoxynivalenol in beer samples with a label-free monolithically integrated optoelectronic biosensor, Journal of Hazardous Materials, 359 (2018) 445–453. [PubMed: 30059886]

[19]. Zhang W, Tang S, Jin Y, Yang C, He L, Wang J, Chen Y, Multiplex SERS-based lateral flow immunosensor for the detection of major mycotoxins in maize utilizing dual Raman labels and triple test lines, Journal of Hazardous Materials, 393 (2020) 122348. [PubMed: 32143157]

[20]. Qin X, Liu J, Zhang Z, Li J, Yuan L, Zhang Z, Chen L, Microfluidic paper-based chips in rapid detection: current status, challenges, and perspectives, TrAC-Trends in Analytical Chemistry, 143 (2021) 116371.

[21]. Xu W, Xiong Y, Lai W, Xu Y, Li C, Xie M, A homogeneous immunosensor for AFB1 detection based on FRET between different-sized quantum dots, Biosensors and Bioelectronics, 56 (2014) 144–150. [PubMed: 24487101]

[22]. Masters BR, Paths to Förster's resonance energy transfer (FRET) theory, The European Physical Journal H, 39 (2014) 87–139.

[23]. Massey M, Wu M, Conroy EM, Algar WR, Mind your P's and Q's: the coming of age of semiconducting polymer dots and semiconductor quantum dots in biological applications, Current Opinion in Biotechnology, 34 (2015) 30–40. [PubMed: 25481436]

[24]. Resch-Genger U, Grabolle M, Cavaliere-Jaricot S, Nitschke R, Nann T, Quantum dots versus organic dyes as fluorescent labels, Nature Methods, 5 (2008) 763–775. [PubMed: 18756197]

[25]. Shimomura O, Johnson FH, Saiga Y, Extraction, purification and properties of aequorin, a bioluminescent protein from the luminous hydromedusan, Aequorea, Journal of cellular and comparative physiology, 59 (1962) 223–239. [PubMed: 13911999]

[26]. Sample V, Newman RH, Zhang J, The structure and function of fluorescent proteins, Chemical Society reviews, 38 (2009) 2852–2864. [PubMed: 19771332]

[27]. Heim R, Cubitt AB, Tsien RY, Improved green fluorescence, Nature, 373 (1995) 663–664.

[28]. Heim R, Prasher DC, Tsien RY, Wavelength mutations and posttranslational autoxidation of green fluorescent protein, Proceedings of the National Academy of Sciences, 91 (1994) 12501–12504.

[29]. Cabantous S, Terwilliger TC, Waldo GS, Protein tagging and detection with engineered self-assembling fragments of green fluorescent protein, Nature Biotechnology, 23 (2005) 102–107.

[30]. Pédelacq J-D, Cabantous S, Tran T, Terwilliger TC, Waldo GS, Engineering and characterization of a superfolder green fluorescent protein, Nature Biotechnology, 24 (2006) 79–88.

[31]. Hamers-Casterman C, Atarhouch T, Muyldermans S, Robinson G, Hammers C, Songa EB, Bendahman N, Hammers R, Naturally occurring antibodies devoid of light chains, Nature, 363 (1993) 446–448. [PubMed: 8502296]

[32]. Greenberg AS, Avila D, Hughes M, Hughes A, McKinney EC, Flajnik MF, A new antigen receptor gene family that undergoes rearrangement and extensive somatic diversification in sharks, Nature, 374 (1995) 168–173. [PubMed: 7877689]

[33]. Liu X, Xu Y, Wan D.-b., Xiong Y, He Z, Wang X, Gee SJ, Ryu D, Hammock BD, Development of a Nanobody–Alkaline Phosphatase Fusion Protein and Its Application in a Highly Sensitive

Direct Competitive Fluorescence Enzyme Immunoassay for Detection of Ochratoxin A in Cereal, Analytical Chemistry, 87 (2015) 1387–1394. [PubMed: 25531426]

[34]. Muyldermans S, Nanobodies: Natural Single-Domain Antibodies, Annual Review of Biochemistry, 82 (2013) 775–797.

[35]. He J, Ma S, Wu S, Xu J, Tian J, Li J, Gee SJ, Hammock BD, Li QX, Xu T, Construction of Immunomagnetic Particles with High Stability in Stringent Conditions by Site-Directed Immobilization of Multivalent Nanobodies onto Bacterial Magnetic Particles for the Environmental Detection of Tetrabromobisphenol-A, Analytical Chemistry, 92 (2020) 1114–1121. [PubMed: 31763820]

[36]. Liu X, Xu Y, Xiong Y, Tu Z, Li Y, He Z, Qiu Y, Fu J, Gee SJ, Hammock BD, VHH Phage-Based Competitive Real-Time Immuno-Polymerase Chain Reaction for Ultrasensitive Detection of Ochratoxin A in Cereal, Analytical Chemistry, 86 (2014) 7471–7477. [PubMed: 24992514]

[37]. He Y, Ren Y, Guo B, Yang Y, Ji Y, Zhang D, Wang J, Wang Y, Wang H, Development of a specific nanobody and its application in rapid and selective determination of Salmonella enteritidis in milk, Food Chemistry, 310 (2020) 125942. [PubMed: 31830714]

[38]. Tang Z, Wang X, Lv J, Hu X, Liu X, One-step detection of ochratoxin A in cereal by dot immunoassay using a nanobody-alkaline phosphatase fusion protein, Food Control, 92 (2018) 430–436.

[39]. Shivkumar MA, Adarsh KS, Inamdar SR, Quantum dot based FRET to cresyl violet: Role of surface effects, Journal of Luminescence, 143 (2013) 680–686.

[40]. Liu J, Mantell J, Di Bartolo N, Jones MR, Mechanisms of Self-Assembly and Energy Harvesting in Tuneable Conjugates of Quantum Dots and Engineered Photovoltaic Proteins, Small, 15 (2019) 1804267.

[41]. Zavrtanik U, Lukan J, Loris R, Lah J, Hadži S, Structural Basis of Epitope Recognition by Heavy-Chain Camelid Antibodies, Journal of Molecular Biology, 430 (2018) 4369–4386. [PubMed: 30205092]

[42]. Sun X, Ji Z, Wei S, Ji Z, Design, Synthesis, and Herbicidal Activity of N-Benzyl-5-cyclopropyl-isoxazole-4-carboxamides, Journal of Agricultural and Food Chemistry, 68 (2020) 15107–15114. [PubMed: 33301336]

Highlights

- A bifunctional and cloneable fluonanobody tracer for ochratoxin A was constructed

- A fluonanobody-based nanosensor *via* FRET for detecting ochratoxin A was developed

- One test could be implemented in a single step within 5 min

- The nanosensor sensitively and selectively detected ochratoxin A down to 5 pg/mL

- The nanosensor is applicable for detecting ochratoxin A in complex food matrices
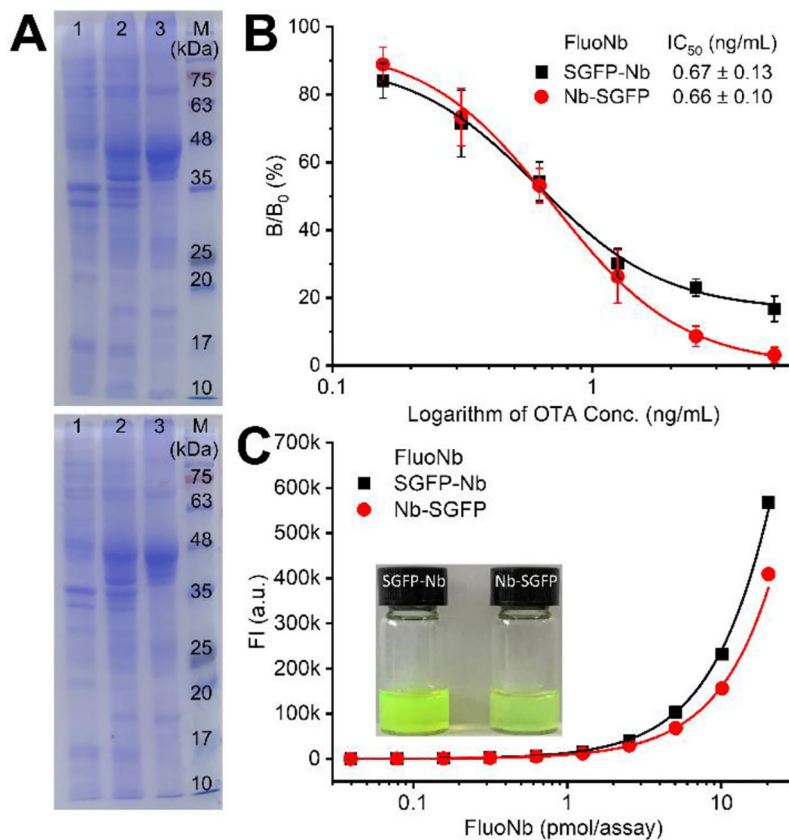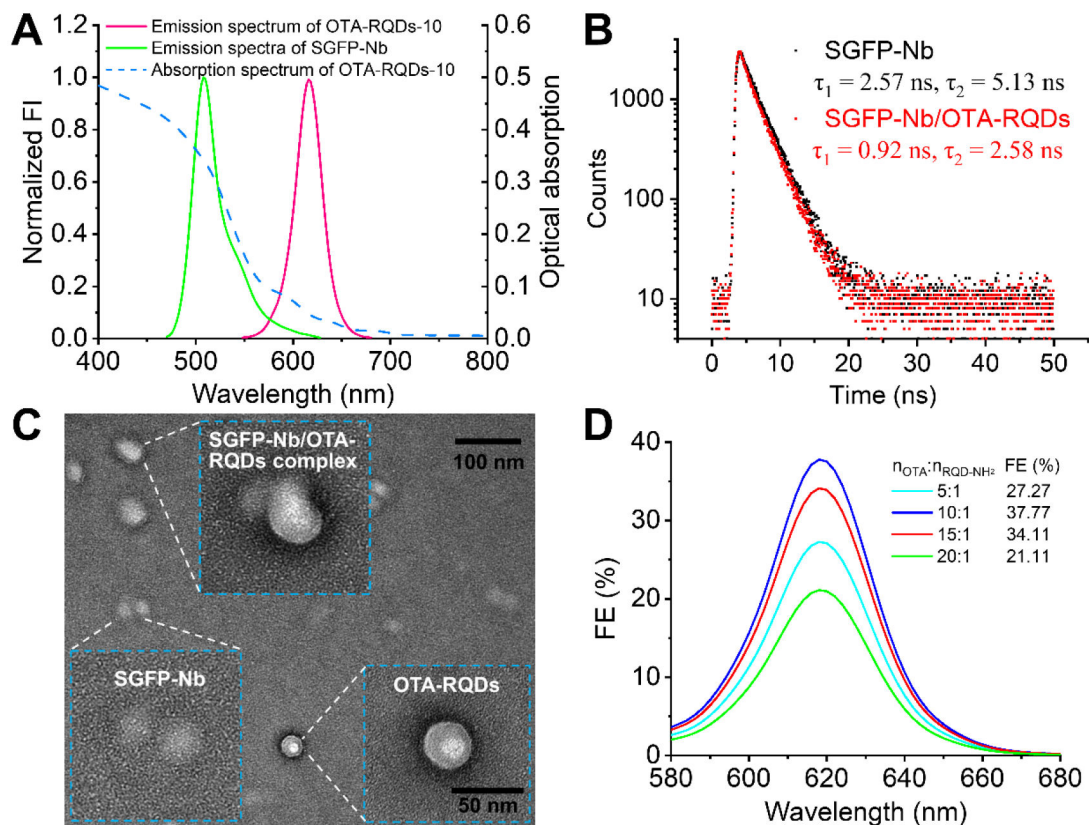
Figure 1.
Analysis of the FluoNbs using SDS-PAGE and ELISA. (**A**) Analysis of the expression of FluoNbs using SDS-PAGE (up: Nb-SGFP, down: SGFP-Nb). Lane M, pre-stained protein molecular weight marker; lane 1, uninduced total bacterial protein; lane 2, induced total bacterial protein; lane 3, bacterial supernatant after ultrasonication. (**B**) Comparison of the antibody activity using an indirect competitive ELISA and (**C**) fluorescent protein activity by measuring the FI at 510 nm (λ_{ex}=485 nm). The error bars denote the SDs of tests conducted in triplicate.
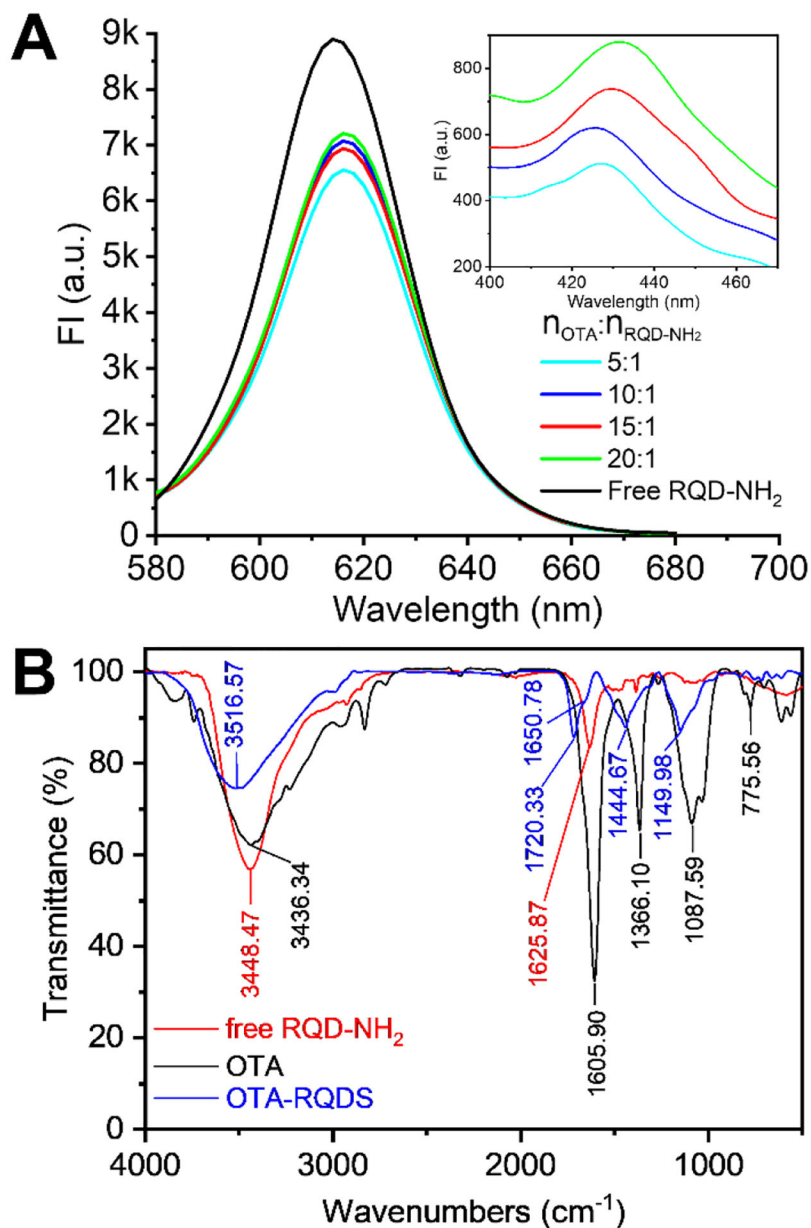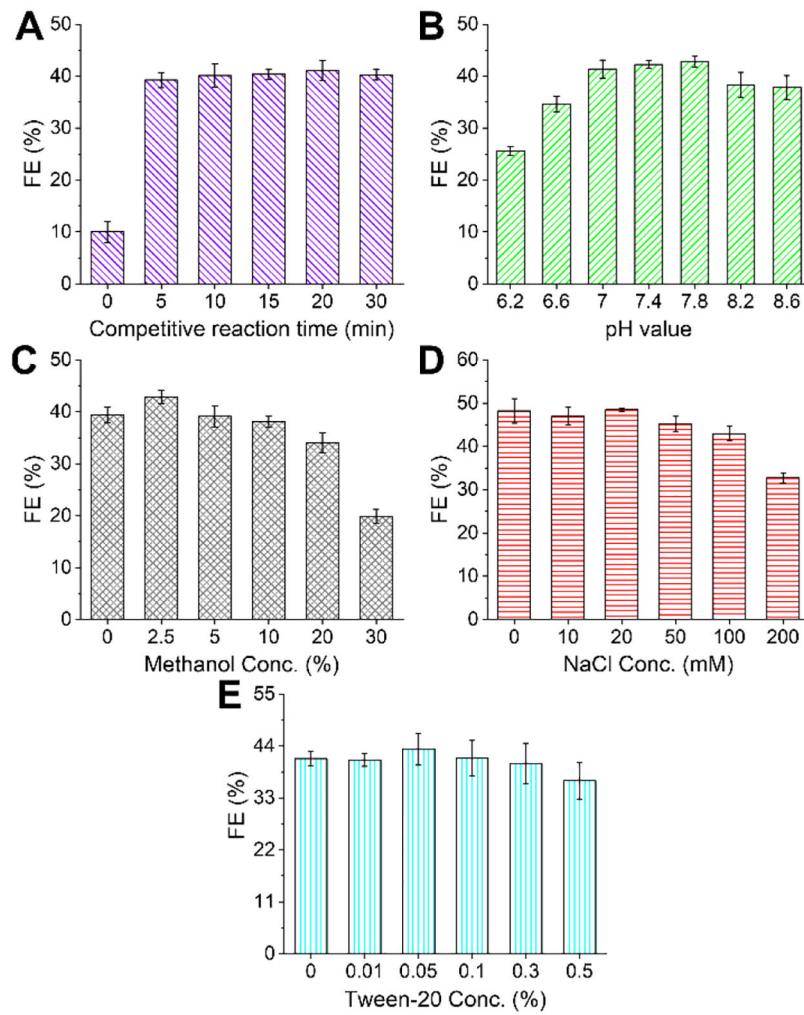
Figure 2.
Optimization and characterization of OTA-RQDs. (**A**) Fluorescence spectrum analysis (λ_{ex}=485 nm) of the OTA-RQDs prepared with diverse input molar ratios. Inset: emission spectra of the OTA-RQDs upon excitation at 365 nm. (**B**) Analysis of the free RQD-NH$_2$ and OTA-RQDs using FTIR.
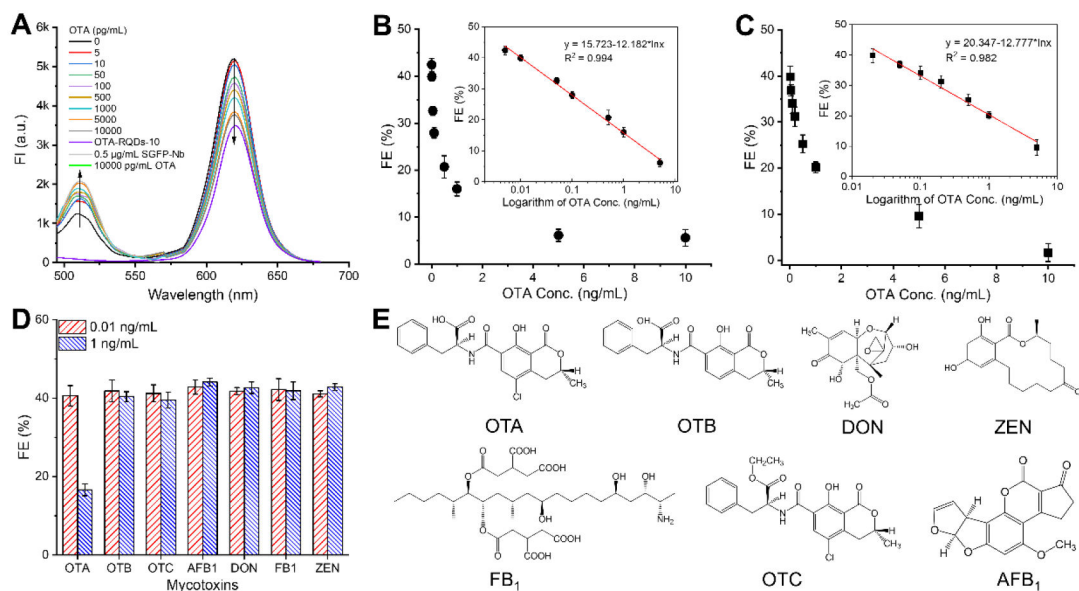
Figure 3.
Feasibility analysis of the FluoNb-based nanosensor for OTA. (**A**) Fluorescence spectrum analysis of the OTA-RQDs-10 (λ_{ex}=530 nm) and SGFP-Nb (λ_{ex}=485 nm) and UV absorption spectrum analysis of the OTA-RQDs-10. (**B**) Fluorescence decay curves of SGFP-Nb in the presence (red curve) and absence (black curve) of OTA-RQDs. λ_{ex}=485 nm and λ_{em}=510 nm; (**C**) Morphology analysis of the SGFP-Nb, OTA-RQDs, and SGFP-Nb/OTA-RQDs complex by negative staining TEM; (**D**) Comparison of the FE values of OTA-RQDs prepared with diverse input molar ratios.
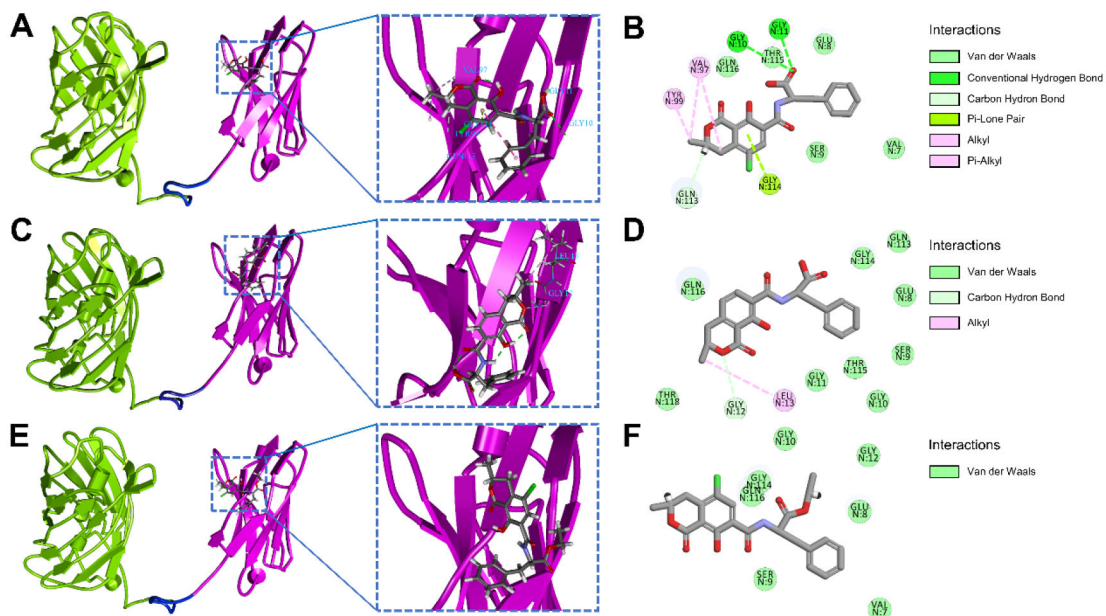
Figure 4.
Optimization of FN-Nanosens. Evaluation of the influence of (**A**) competitive incubation time, (**B**) pH, (**C**) methanol, (**D**) ion strength, and (**E**) Tween-20 on the performance of FN-Nanosens. The error bars denote the SDs of tests conducted in triplicate.

Figure 5.
Analytical performance of FN-Nanosens and EN-Nanosens. (**A**) Fluorescence emission spectra (λ_{ex}=485 nm) of the mixture of SGFP-Nb, OTA-RQDs-10, and a series of OTA standards, and the control groups of separate OTA-RQDs-10, 0.5 μg/mL SGFP-Nb, and 10000 pg/mL OTA. (**B**) The calibration curve fitted by plotting the FE value *versus* the OTA concentration for FN-Nanosens. Inset: the linear portion of the curve fitted with the FE value against the logarithm of OTA concentration. (**C**) The calibration curve fitted by plotting the FE value *versus* the OTA concentration for EN-Nanosens. Inset: the linear portion of the curve fitted with the FE value against the logarithm of OTA concentration. (**D**) Cross-reactivity of FN-Nanosens with analogs of OTA and several typical cereal mycotoxins. (**E**) Chemical structures of AFB$_1$, DON, FB$_1$, OTA, OTB, OTC, and ZEN. The error bars denote the SDs of tests conducted in triplicate.

Figure 6.
Molecular docking results of SGFP-Nb and three ochratoxins. Docking model results and close-up views of the complexes of SGFP-Nb + OTA (**A**), SGFP-Nb + OTB (**C**), and SGFP-Nb + OTC (**E**). Two-dimensional diagrams between amino acid residues of SGFP-Nb + OTA (**B**), SGFP-Nb + OTB (**D**), and SGFP-Nb + OTC (**F**).
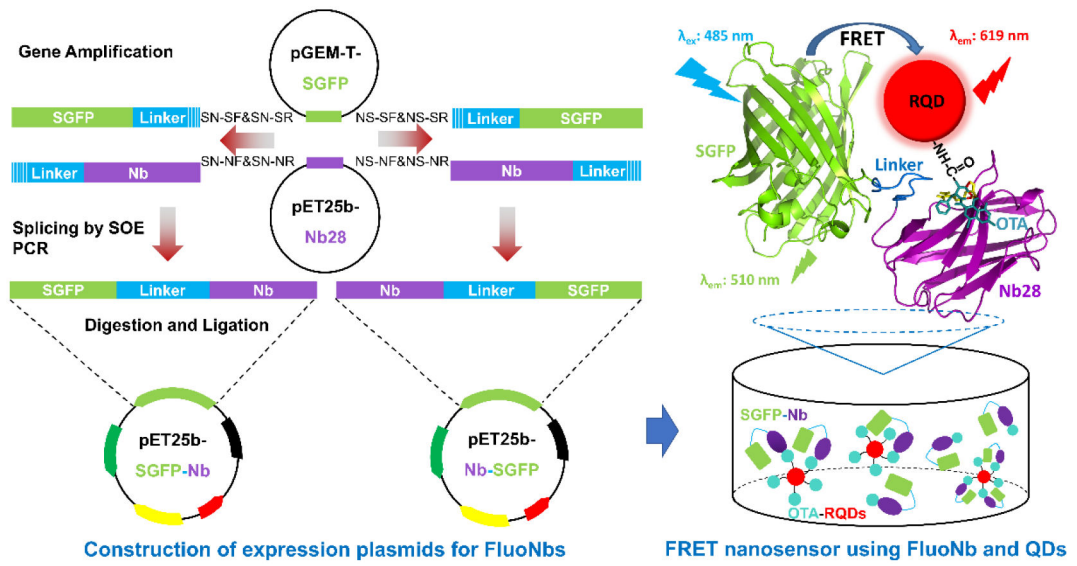
Scheme 1.
Schematic diagram of the FRET-mediated nanosensor designed using Nb-SGFP and QDs, for detection of OTA.

Table 1.

Docking energy of SGFP-Nb and three ochratoxins.

	OTA	OTB	OTC
-CDOCKER interaction energy (kcal/mol)	35.29	20.49	21.58

Table 2.

Recoveries of OTA from the spiked cereal samples tested using FN-Nanosensor.

Sample	Spiking level (µg/kg)	Intra-assay[a]		Inter-assay[b]	
		Recovery ± SD (%)	RSD (%)	Recovery ± SD (%)	RSD (%)
Rice	0.02	85 ± 7	8	87 ± 10	12
	0.2	109 ± 9	8	100 ± 11	11
	2	98 ± 4	4	104 ± 3	3
Oats	0.02	94 ± 14	15	82 ± 9	11
	0.2	72 ± 8	11	73 ± 10	14
	2	70 ± 4	5	84 ± 3	3
Barley	0.02	93 ± 11	12	83 ± 13	16
	0.2	91 ± 8	9	85 ± 8	9
	2	105 ± 6	6	106 ± 10	9
Wheat	0.02	85 ± 6	7	76 ± 6	8
	0.2	74 ± 5	7	80 ± 4	5
	2	88 ± 14	16	88 ± 3	3

[a]Each assay was performed in triplicate on the same day.

[b]Each assay was performed in triplicate on three days.

Author Manuscript

Author Manuscript

Author Manuscript

Author Manuscript

Table 3.

Analysis of OTA content in cereal samples.

Sample[a]	LC-MS/MS[b] (µg/kg)	FN-Nanosens (µg/kg)
B1	1.83 ± 0.14	1.69 ± 0.10
B2	ND[c]	ND
O1	0.82 ± 0.10	1.92 ± 0.14
O2	7.53 ± 0.11	6.53 ± 0.65
O3	12.0 ± 0.30	13.3 ± 1.07
O4	ND	ND
O5	1.22 ± 0.04	1.40 ± 0.12
R1	2.03 ± 0.09	2.47 ± 0.24
R2	ND	ND
R3	1.80 ± 0.17	1.59 ± 0.12
R4	1.45 ± 0.18	1.34 ± 0.14
W1	ND	0.13 ± 0.02
W2	ND	ND

[a]B, O, R, and W represent barley, oats, rice, and wheat, respectively.

[b]The LOD of the LC-MS/MS method was 0.01 ng/mL [33].

[c]Not detected.